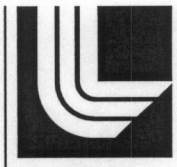

LAWRENCE
LIVERMORE
NATIONAL
LABORATORY

UCRL-JC-153901

Electrical Resistivity as an Indicator of Saturation in Fractured Geothermal Reservoir Rocks: Experimental Data and Modeling

R.L. Detwiler, J.J. Roberts

June 23, 2003

Geothermal Resources Council 2003 Annual Meeting,
Morelia, Mexico, October 12-15, 2003

This work was performed under the auspices of the U.S. Department of Energy by University of California, Lawrence Livermore National Laboratory under Contract W-7405-Eng-48.

ELECTRICAL RESISTIVITY AS AN INDICATOR OF SATURATION IN FRACTURED GEOTHERMAL RESERVOIR ROCKS: EXPERIMENTAL DATA AND MODELING

Russell L. Detwiler and Jeffery J. Roberts

Lawrence Livermore National Laboratory
P.O. Box 808, L-201
Livermore, CA 94551
e-mail: detwiler1@llnl.gov

Key Words: hydraulic testing, fracture-matrix interaction, two-phase flow, phase change, resistivity

ABSTRACT

The electrical resistivity of rock cores under conditions representative of geothermal reservoirs is strongly influenced by the state and phase (liquid/vapor) of the pore fluid. In fractured samples, phase change (vaporization/condensation) can result in resistivity changes that are more than an order of magnitude greater than those measured in intact samples. These results suggest that electrical resistivity monitoring of geothermal reservoirs may provide a useful tool for remotely detecting the movement of water and steam within fractures, the development and evolution of fracture systems and the formation of steam caps. We measured the electrical resistivity of cores of welded tuff containing fractures of various geometries to investigate the resistivity contrast caused by active boiling and to determine the effects of variable fracture dimensions and surface area on water extraction from the matrix. We then used the Nonisothermal Unsaturated Flow and Transport model (NUFT) (Nitao, 1998) to simulate the propagation of boiling fronts through the samples. The simulated saturation profiles combined with previously reported measurements of resistivity-saturation curves allow us to estimate the evolution of the sample resistivity as the boiling front propagates into the rock matrix. These simulations provide qualitative agreement with experimental measurements suggesting that our modeling approach may be used to estimate resistivity changes induced by boiling in more complex systems.

INTRODUCTION AND BACKGROUND

Evaluating the effectiveness and sustainability of geothermal energy production strategies requires understanding how hydraulic stresses influence permeability and phase distribution within the reservoir. The hydraulic response of a reservoir to withdrawal and injection of fluids provides one measure of reservoir performance, but hydraulic data provides limited insights into intra-well details, such as fracture density and orientation, and phase distribution. Electrical techniques such as cross-well EM, electrical resistivity tomography, and the long spacing induction tool (GeoBILT) (Mallan et al., 2002; Wilt et al., 1997) have the potential to complement hydraulic production data by providing quantitative measures of evolving reservoir properties. However, effective implementation of these techniques requires the ability to correlate measurements of electrical resistivity with changes in properties of interest such as fracture density and fluid saturation.

Electrical resistance is sensitive to properties of both the host rock (surface conduction, pore-size distribution, and the density of fractures) and the pore fluid (temperature, pressure, chemical composition, and phase distribution) (e.g., Brace et al., 1965; Walsh and Brace, 1984; Roberts et al., 2001a). The sensitivity of electrical resistance to such a wide range of variables makes it difficult to predict quantitatively the electrical response of a geothermal reservoir. However, the relative changes in resistivity caused by reservoir production, reinjection, and fracturing can provide valuable insights into the evolution of the host rock and resident fluids.

Using changes in resistivity (ρ) to infer changes in fracture density and/or phase saturation requires an effective model of ρ as a function of phase saturation (S), fluid temperature (T), and fluid pressure (P). We have designed a series of laboratory experiments to evaluate a model for $\rho(S,T)$ presented by Roberts et al., (2001b). Because it is difficult to reliably measure saturation distribution within samples under reservoir conditions (high P and T), we evaluate the model of $\rho(S,T)$ by combining systematic experiments with numerical simulations of fluid flow and phase change to predict the corresponding changes in ρ. Evaluating and refining computational models for these lab-scale experiments will provide insights into which parameters and processes are important when interpreting field-scale electrical data.

EXPERIMENTAL PROCEDURE

Samples and Preparation

Multiple samples were prepared from the same core of welded tuff. Welded tuff provides a good analog to many common geothermal reservoir rocks in that it has very low matrix permeability ($\sim 10^{-18}$ m^2; $\sim$1 μD). Furthermore, the hydraulic properties of the welded tuff used in our experiments have been thoroughly characterized (e.g., Flint, 2003). The samples were prepared by machining right-circular cylinders 2.5 cm long and 2.5 cm diameter. Analog fractures were created in each sample by drilling a hole through the axis of each sample. Three different sample configurations were prepared having small, medium, and large sized holes (TS, TM, and TL), with diameters of 0.16, 0.42, and 0.65 cm, respectively. While the holes in the samples exhibited different geometry than a fracture,

they provided a similar dominant flow path through each sample with a simplified flow geometry to facilitate comparison with model predictions. The end caps were designed to allow flow to enter and exit the samples only through the holes. Thus, all flow into and out of the rock matrix was radial flow to or from the hole. The ends of each sample were sputter-coated with gold to help ensure good electrical connection between the rock and the end caps. Porosity was determined by subtracting dry density from wet density. Dried and evacuated samples were immersed in a solution of high-purity NaCl and degassed, distilled water (1.65 g/l NaCl). Fluid resistivity at room temperature was ~6.4 Ω-m (conductivity = 1.53 mS/cm).

Experimental Apparatus

The apparatus consists of an externally heated pressure vessel with separate pumps and controls for confining pressure and pore pressure on either end of the sample (Figure 1). Roberts et al. (2001a) provide a complete description of the experimental apparatus and measuring procedures. Pore pressure was controlled independently between 0 and 3.6 MPa with two syringe pumps capable of accurately controlling pressure, flow rate, or volume. An impedance bridge was used to measure the resistance of the electrically isolated samples at 1 kHz. Electrical resistivity was calculated from the resistance and geometry of the core. Temperature was measured with two type T thermocouples with an accuracy of ±2°C. One thermocouple was placed in the confining fluid near the sample and the other protruded through the end cap partway into the hole in the sample to measure the transient response of the pore fluid temperature during phase changes. Resistivity measurements have been made at temperatures up to 275 C. Data collection was automated using a scanning unit and microcomputer.

<Place Figure 1 here>

Experimental procedures

After placing each sample in the pressure vessel, the pore and confining pressures were raised to 1.15 and 3.59 MPa, respectively. The temperature of the samples was controlled at 166 C. At this temperature and pressure, the transition from liquid to vapor occurs at 0.72 MPa. Three different experiments were conducted on each of the cores: 1) a constant pressure test, 2) a shut-in test, and 3) a drawdown test (Detwiler et al., 2003). Each of these tests imposed different hydraulic boundary conditions on the sample resulting in different electrical response during each test. The constant pressure test involved instantaneously lowering the pore pressure to 0.46 MPa and controlling the pore pressure at this pressure for the duration of the experiment. The shut-in test was initiated by instantaneously lowering the pore pressure to 0.46 MPa, controlling the pressure for 30 seconds and then isolating the sample from the pressure control system. A pressure transducer measured the subsequent rise in pressure caused by fluid migrating from the rock matrix towards the hole. During the drawdown test, a constant volumetric flow rate of 0.003 ml/min was withdrawn from the sample causing gradual pore pressure reduction.

ELECTRICAL RESISTIVITY RESULTS AND DISCUSSION

Effects of Fractures on Resistivity

Roberts (2001) measured values of ρ at S=1 in welded tuff samples with similar porosity from the same outcrop. We combined their model of $\rho_{matrix}(S)$ with the Arrhenius relationship:

$$\sigma = \sigma_o \exp(-Ea/kT) \qquad (1)$$

where conductivity (σ) = 1/ρ, Ea is the activation energy, k is the Boltzmann constant, and T is the temperature to estimate ρ_{matrix} under our experimental conditions. We also calculated the value of ρ for the saturated hole in each experiment (ρ_{hole}) using the calculated conductivity of the saturating fluid at 166 C (0.74 S/m). Table 1 compares estimates of ρ_o for each sample with the measured value at the beginning of each experiment. Also, because we are interested primarily in changes in ρ caused by phase change within the sample, we compare modeled values of ρ/ρ_o immediately after boiling the liquid in the hole for each of the samples with measured values. The measured values of ρ were taken to be the value of ρ measured immediately after the pressure drop caused the fluid in the hole to vaporize, effectively eliminating the conductive pathway through the hole. The modeled values were calculated by assuming that conduction occurred only through the matrix. The modeled ratio of ρ/ρ_o includes the effects of a metallic-sheathed thermocouple extending into the hole and an additional series resistance at the electrode when

boiling was initiated.

<insert Table 1 here>

The results in Table 1 demonstrate that we can predict the initial values of ρ reasonably well for these experiments. We now consider the transient response of ρ as the boiling front propagates through the rock matrix under the differing hydraulic boundary conditions. **Figure 2** shows ρ/ρ_o plotted against time for six of the constant pressure tests. Immediately after lowering the pressure in each sample (t=0), ρ/ρ_o increased due to boiling of the liquid in the hole. The magnitude of the jump in ρ/ρ_o reflects the relative cross-sectional area of the hole in each sample. Vaporization of the liquid in the hole causes a decrease in temperature of ~20 to 30 C, however, the thermocouple readings confirm that the temperature in the sample recovers to equilibrium (166 C) much more quickly than the pressures and resistivities reach steady state. This suggests that measured values of ρ reflect changes in saturation rather than the short-lived temperature fluctuation. After the initial increase, ρ/ρ_o gradually increases as the boiling front induced by the reduced pressure in the hole propagates into the matrix. For each of the samples, ρ/ρ_o exhibits a log-linear increase until the phase distribution within the sample nears equilibrium, at which point the rate of change in ρ/ρ_o begins to decrease.

<Place Figure 2 here>

To evaluate the reproducibility of the experiments and variability between samples, we repeated the constant pressure test in three different large-hole samples (TL_2, TL_12, and TL_13). In TL_13, we conducted two constant pressure tests (TL_13_1 and TL_13_2) separated by a period of approximately 5 weeks during which the sample remained at elevated pressure and temperature. The plots of ρ/ρ_o demonstrate that the magnitude of the initial relative increase caused by boiling in the hole is influenced considerably more by the cross-sectional area of the hole in the sample than by variability between tests and samples with the same size hole. However, the transient response of ρ/ρ_o as the boiling front propagates into the rock matrix exhibits significant variability between samples and tests within the same sample.

Figures 3 shows P/P_{boil} and ρ/ρ_o (where P is the pressure in the hole and P_{boil} is the phase transition pressure at 166 C) plotted against time for the shut-in tests in samples TS_7 and TL_12. As with the constant pressure tests, when the pressure is dropped at the start of the test, the liquid in the hole changes to steam, and the resistivity rises. However, because the sample is isolated from the pressure control system after 30 seconds, fluid migrating from the rock into the hole causes the pressure in the hole to rise. The pressure in the large-hole sample (TL_12) appears to reach steady state more quickly than for the small hole. However, the continued increase in ρ/ρ_o suggests that the distribution of liquid and vapor in the pore space of the rock matrix has not fully equilibrated. Furthermore, in TS_7, fluid migrating from the rock matrix into the hole caused the pressure to rise above P_{boil}, whereas in TL_12, the pressure leveled off at P_{boil}. This indicates that in TS, the fluid in the hole condensed due to flow from the matrix, but in TL_12 remained as vapor.

Figures 4a and 4b show P/P_{boil} and ρ/ρ_o, respectively, plotted against dimensionless time (t') for the drawdown tests in samples TS_7, TM_8, and TL_12; $t' = tQ/V$, where t is time, Q is the volumetric flow rate from the sample, and V is the volume of the hole. For each test, t' was set to zero at the time the pressure in the hole reached P_{boil} to facilitate direct comparison of the experiments. For a non-porous rock matrix and a hole filled with an ideal gas, the steady volumetric extraction of fluid from the hole would result in similar reductions in pressure with t'. This suggests that the different responses of P/P_{boil} exhibited in Figure 4a for each sample result from the different rates of fluid flow from the rock matrix in response to pumping from the hole. Thus, for sample TS_7, though the hole in the sample has a smaller diameter than the hole in sample TL_12, the relative rate of drawdown in the hole is slower in sample TS_7. This is reflected in the measurements of ρ/ρ_o, which demonstrate that a two order of magnitude increase in ρ/ρ_o occurs at t'~0.04 in sample TL_12 and t'~0.8 in sample TS_7.

<Place Figure 4 here>

<Place Figure 5 here>

COMPUTATIONAL MODELLING

We combine numerical modeling of fluid flow and phase change within the samples with a model of $\rho(S,T)$ to predict the transient response of ρ in our experiments. Previous experiments designed to quantify the relationship between liquid saturation, S, and ρ have yielded a model of $\rho(S)$ (Roberts, 2001) at temperatures up to 95 C. This relationship was found to represent ρ well for S greater than ~0.15 - 0.2. Subsequently, Roberts et al. (2001b) used (1) to extend this relationship to temperatures above 100 C to estimate electrical resistivities in a field-scale experiment. To test the ability of the proposed model of $\rho(S,T)$ to effectively track the transient changes in ρ/ρ_o observed in our experiments, we used the Nonisothermal Unsaturated Flow and Transport model (NUFT) (Nitao,1998) to simulate fluid migration and phase change induced by the experimental boundary conditions. We then calculated the transient response of ρ using the proposed $\rho(S,T)$ model. We present results focused on the constant pressure tests presented in **Figure 2**.

Parameters used to describe the mass and heat transport properties of the rock matrix were independently measured for cores from the same layer within the same formation as the samples used for the current experiments. The hole was assigned separate material properties selected to represent an empty hole. The values of parameters used for the simulations are summarized in **Table 2.**

<insert Table 2 here>

Figure 5 shows simulated saturation profiles for a small- and large-hole sample at a sequence of times. The liquid saturation decreases as the pressure drop propagates into the rock matrix and steam flows towards the hole. As expected, the time-scale required to reach a steady-state saturation distribution is longer for the sample with the smaller hole due to a smaller surface area between the hole and the rock matrix.

<Place Figure 5 here>

Figure 6 compares simulated values of ρ/ρ_o for the small- and large-hole samples to the experimentally measured data. The simulations exhibit good qualitative agreement with the experimental results presented in **Figure 2**. As quantified in Table 1, the initial increase in ρ/ρ_o caused by boiling the fluid in the hole at t~0 is similar for both samples. The rate of increase and the final value of ρ/ρ_o are underestimated for the small-hole sample, however, the multiple experimental realizations shown for the large-hole sample suggest that the magnitude of the discrepancy may be smaller than the magnitude of experimental variability. The simulations transition quickly from increasing ρ/ρ_o to a steady value, whereas the experiments appear to asymptotically approach a steady value. This may be due to pore-scale redistribution of the fluid in the rock matrix, which can result in measurable changes in ρ, especially at low saturations, but are not explicitly calculated by continuum models.

CONCLUSIONS

The ability to infer hydraulic behavior from electrical measurements in the field is based upon the relationship between electrical resistance and properties such as saturation, temperature, and pressure. Understanding the interaction of these variables and their influence on numerical simulations at the laboratory scale is fundamental to interpreting larger scale field data. We have presented results from a systematic series of laboratory experiments specifically designed to test our ability to simulate flow, phase distribution, and electrical response under conditions typical of geothermal reservoirs. Preliminary modeling results demonstrate qualitative agreement with the experimental results. More extensive simulations over the full range of experimental boundary conditions should help to clarify sources of discrepancies between experiments and simulations. Additionally, sensitivity studies in which model parameters are systematically varied will shed light on the relative importance of the many parameters involved in modeling two-phase flow in geothermal systems and their role in estimating field-scale changes in electrical resistivity.

ACKNOWLEDGMENTS

D. Ruddle helped prepare samples and provided valuable technical assistance. S. Carlson and C. Talaber provided essential technical support and expertise. We thank P. Kasameyer for fruitful discussion and comments. This work

was supported by the Office of Geothermal and Wind Technology, under the Assistant Secretary for Energy Efficiency and Renewable Energy of the U.S. Department of Energy, and the Office of Basic Energy Science. This work was performed under the auspices of the U. S. Department of Energy by the University of California, Lawrence Livermore National Laboratory under Contract No. W-7405-Eng-48.

REFERENCES

Detwiler, R. L., J. J. Roberts, W. Ralph, and B.P. Bonner (2003), Modeling Fluid Flow and Electrical Resistivity in Fractured Geothermal Reservoir Rocks, Proceedings, *Twenty Eighth Annual Stanford Geothermal Reservoir Engineering Workshop*, January 27-29, Stanford, CA, SGP-TR-173, 301-306.

Duba, A., Piwinskii, A. J., Santor, M., and Weed, H. C. (1978), "The Electrical Conductivity of Sandstone, Limestone and Granite," *Geophys. J. R. Astron. Soc.*, **53**, 583–597.

Haas, J. L. Jr. (1971), "The Effect of Salinity on the Maximum Thermal Gradient of a Hydrothermal System at Hydrostatic Pressure," *Economic Geol.*, **66**, 940–946.

Keller, G.V. (1966). Electrical properties of rocks and minerals. In: Handbook of Physical Constants (Edited by S. P. Clark, Jr.), Memoir 97, Geological Society of America, New York, New York, USA.

Lin, W., Daily, W.D. (1984), Transport properties of Topopah Spring tuff, , *Lawrence Livermore National Lab. Rep., UCRL-JC-53602.*

Llera, F. J., Sato, M., Nakatsuka, K., and Yokoyama, H. (1990), "Temperature Dependence of the Electrical Resistivity of Water-Saturated Rocks," *Geophysics*, **55**, 576–585.

Murray, L. E., Rohrs, D. T., Rossknect, T. G., Aryawijawa, R., and Pudyastuti, K. (1995), "Resource Evaluation and Development Strategy, Awibengkok Field," Proceedings World Geothermal Congress, Florence, Italy, pp. 1525–1531.

Roberts, J. J. (2001), Electrical properties of microporous rock as a function of saturation and temperature, *J. Applied Phys., 21*, 1687-1694.

Roberts, J. J., Bonner, B. P., and Duba, A. G. (2000), "Electrical Resistivity Measurements of Andesite and Hydrothermal Breccia from the Awibengkok Geothermal Field, Indonesia," *TwentyFifth Annual Stanford Geothermal Reservoir Engineering Workshop*, 339-344.

Roberts, J. J., Duba, A. G., Bonner, B. P., and Kasameyer, P. (2001a), "Resistivity During Boiling in the SB-15-D Core from The Geysers Geothermal Field: The Effects of Capillarity," *Geothermics, 30*, 235-254.

Roberts, J. J., A. Ramirez, S. Carlson, W. Ralph, W. Daily, and B. P. Bonner (2001b), Laboratory and field measurements of electrical resistivity to determine saturation and detect fractures in a heated rock mass, *Geothermal Resources Council, Transactions, 25*, 681-686.

Table 1: Summary of changes in resistivity due to boiling: Experimental and modeled

	Experimental		Modeled	
Sample ID	**ρ_o, ohm m**	**ρ/ρ_o**	**ρ_o, ohm m**	**ρ/ρ_o adjusted***
TS_7	56	2.56	96	2.29
TM_8_1	28	5.41	37	7.94
TM_8_2	22	6.39	37	7.94
TM_9	24	7.94	37	7.94
TL_2	11	16.89	18	17.04
TL_10	12	23.83	18	17.04
TL_12	8	24.62	18	17.04
TL_13	13	21.70	18	17.04

***adjusted for effect of TC in hole and endcap resistance upon boiling**

Table 2: Summary of model parameters

Parameter	**Rock matrix**	**Hole**
K – permeability (m^2)	7.2e-18	1.0e-6
ϕ - porosity	0.157	1.0
c_p – specific heat (J/kg C)	1040	N/A
ρ_b (kg/m^3)	2513	N/A
Thermal conductivity (W-m/ C)		
solid	1.74	N/A
liquid	2.34	2.34
vapor	1.74	1.74
S_r - residual saturation	0.07	1.0e-5
m - van Genuchten param.	0.29	0.5
α - van Genuchten param. (1/Pa)	1.14e-5	.00114
Δr – grid spacing (m)	2.0e-4	2.0e-4

Figure Captions

Figure 1. Schematic of apparatus. Sample is electrically isolated and held in an externally heated pressure vessel with separate reservoirs, pumps, and controls for confining and pore pressure. Type J thermocouples (TC) measure temperature of the three-zone heater and at two locations adjacent to the sample. An impedance bridge (LCR meter, HP4284a) is used to measure the electrical properties of the sample. A microcomputer controls the experiment and data collection. A second set of pore pressure pumps (not shown) permit accurate determination of flow rate through samples.

Figure 2. ρ/ρ_o for constant pressure tests conducted in five different samples.

Figure 3. P/P_{boil} (top) and ρ/ρ_o (bottom) for shut-in tests in samples TL-12 and TS-7.

Figure 4. P/P_{boil} (top) and ρ/ρ_o (bottom) for drawdown tests in samples TL-12 and TS-7.

Figure 5. Simulated saturation profiles at different times for a large-hole sample (top) and small-hole sample (bottom).

Figure 6. Simulated ρ/ρ_o (solid lines) compared to measured ρ/ρ_o (dashed lines) for small- and large-hole samples during a constant pressure test.

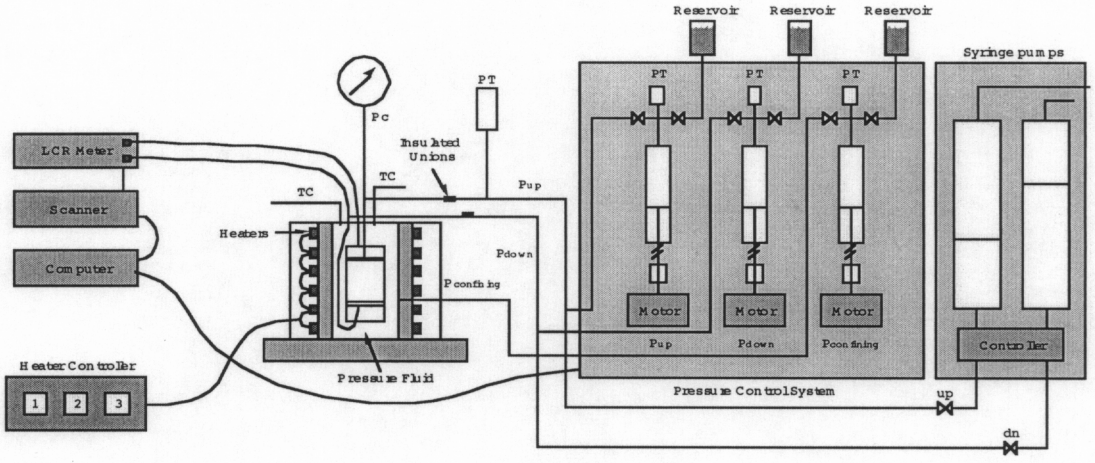

Figure 1.

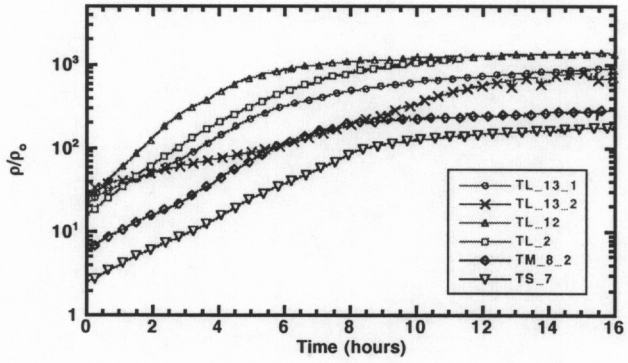

Figure 2.

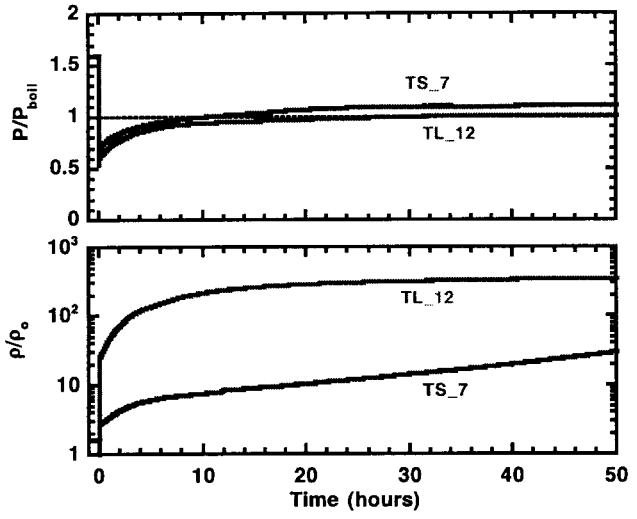

Figure 3.

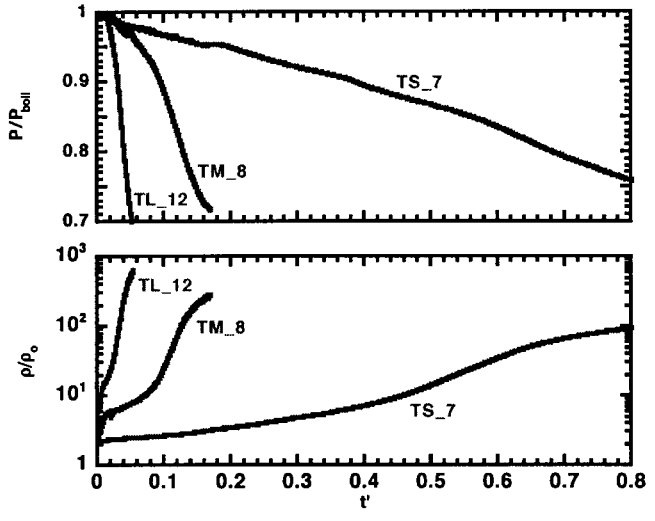

Figure 4.

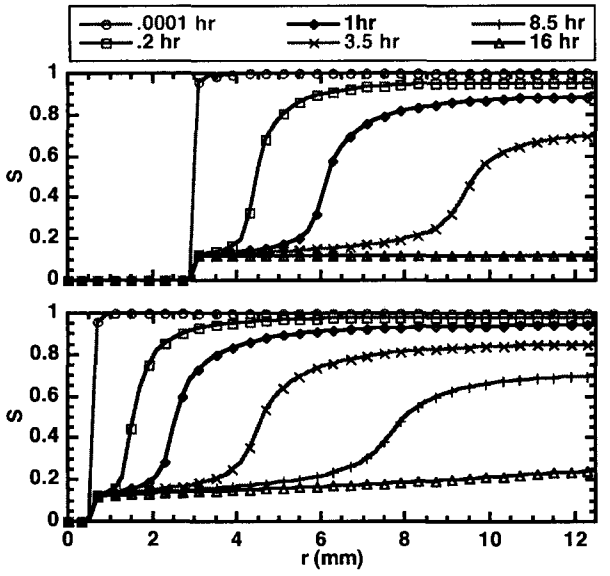

Figure 5.

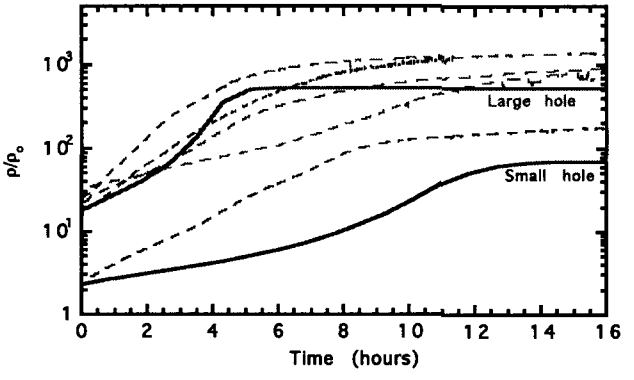

Figure 6.